Applied Catalysis A: General 433–434 (2012) 243–250

Contents lists available at SciVerse ScienceDirect

Applied Catalysis A: General

journal homepage: www.elsevier.com/locate/apcata

Highly dispersed supported ruthenium oxide as an aerobic catalyst for acetic acid synthesis

Anders B. Laursen[a,*], Yury Y. Gorbanev[b], Filippo Cavalca[c], Paolo Malacrida[a], Alan Kleiman-Schwarsctein[a], Søren Kegnæs[b], Anders Riisager[b], Ib Chorkendorff[a], Søren Dahl[a,**]

[a] Center for Individual Nanoparticle Functionality (CINF), Department of Physics, Technical University of Denmark (DTU), Fysikvej Build. 307, DK-2800 Kgs. Lyngby, Denmark
[b] Centre for Catalysis and Sustainable Chemistry (CSC), Department of Chemistry, Technical University of Denmark (DTU), Kemitorvet Build. 207, DK-2800 Kgs. Lyngby, Denmark
[c] Center for Electron Nanoscopy (CEN), Technical University of Denmark (DTU), Fysikvej Build. 307, DK-2800 Kgs. Lyngby, Denmark

ARTICLE INFO

Article history:
Received 13 December 2011
Received in revised form 17 May 2012
Accepted 19 May 2012
Available online 29 May 2012

Keywords:
Heterogeneous catalysis
Ruthenium oxide
Aerobic ethanol oxidation
RuO_4
Support effects
High-loading catalysts
Ru(VI) oxide

ABSTRACT

The increasing need for shifting to renewable feedstocks in the chemical industry has driven research toward using green aerobic, selective oxidation reactions to produce bulk chemicals. Here, we report the use of a ruthenium mixed oxide/hydroxide (RuO_x) on different support materials for the selective aerobic oxidation of ethanol to acetic acid. The RuO_x was deposited onto different oxide supports using a new gas-phase reaction, which in all cases resulted in homogeneous nanoparticulate films. The RuO_x particle size ranged from 0.3 to 1.5 nm. The catalytic activity was evaluated on TiO_2, $Mg_6Al_2(CO_3)(OH)_{16} \cdot 4(H_2O)$, $MgAl_2O_4$, $Na_2Ti_6O_{13}$ nanotubes, ZnO, γ-Al_2O_3, WO_3, CeO_2, and $Ce_{0.5}Zr_{0.5}O_2$ supports. The CeO_2 supported RuO_x had the highest activity, and selectivity toward acetic acid, of all the materials when normalized with respect to Ru-loading. This high activity was independent of the surface area of the support and the loading of RuO_x under the tested conditions. This was attributed to the highly uniform size of the RuO_x deposits, demonstrating that the deposition is suitable for producing small nanoparticles at high loadings. To elucidate the reason for the promotional effect of CeO_2, $Ce_{0.5}Zr_{0.5}O_2$ was investigated as a high oxygen storage capacity support, however, this did not result in higher catalytic activity. The high activity of CeO_2 supports compared to the low activity ZnO appear correlated to the presence of high valence Ru(VI) species analogous to that observed in literature.

1. Introduction

The need for synthesizing bulk chemicals from non-fossil alternative feedstock rather than fossil resources increases as the latter becomes more scarce. This production of bulk chemicals should be as benign as possible for the environment, or "green" [1]. One such bulk chemical is acetic acid, which is produced on the millions of tonnes scale worldwide from syngas, butane, and naphtha [2]. The production of biomass-derived ethanol or "bio-ethanol" has increased dramatically since the late 1990s [3]. This bio-ethanol could find use as a versatile, sustainable chemical feedstock for the green production of "bio-acetic acid" [4].

Selective partial oxidation of organic molecules has attracted increasing attention over the past decade, especially using molecular oxygen, i.e. aerobic oxidation [5–14]. Aerobic oxidation is considered to be a "green" process because the only by-product is water, unlike the use of classic metal oxide oxidants, which generate stoichiometric amounts of metal waste [15,16]. Furthermore, aerobic oxidation is also attractive due to the low cost of ubiquitous oxygen.

RuO_2 is perhaps most well known as the archetypical electrocatalyst for the oxygen evolution reaction (OER) [17]. Several reactions are also reported in literature to be catalyzed by ruthenium-based catalysts, e.g. ammonia synthesis/decomposition [18], metathesis reactions [19], dehydrogenation of ethane [20], and oxidation reactions [21]. The number of reports on heterogeneous ruthenium-based aerobic oxidation catalysts are limited, and primarily focused on the oxidation of alcohols to oxo compounds in organic solvents [5,22–25], and in aqueous solution [26–28]. In this work we focus on the green selective aerobic oxidation of ethanol (CH_3CH_2OH) to acetic acid (CH_3COOH) in aqueous solution.

Recently, we reported a new procedure for the conformal coating of metal oxide supports with a high coverage of ruthenium oxide (RuO_x) nanoparticles [29]. The RuO_x deposited on TiO_2 and WO_3, according to this procedure, showed good results as OER catalysts for electrocatalytic and photoelectrocatalytic water splitting, respectively. It was demonstrated that the nanoparticles covered

* Corresponding author. Tel.: +45 45253139.
** Principal corresponding author. Tel.: +45 45253192.
E-mail addresses: ablaursen.chemistry@gmail.com (A.B. Laursen), soren.dahl@fysik.dtu.dk (S. Dahl).

0926-860X/$ – see front matter © 2012 Elsevier B.V. All rights reserved.
http://dx.doi.org/10.1016/j.apcata.2012.05.025

the support in very thin and homogeneous layers, providing a high dispersion of the RuO_x nanoparticles.

In the present work the catalytic properties of this novel type of heterogeneous catalyst was investigated for the selective aerobic oxidation of ethanol. To evaluate the support effect on the catalytic activity, the active RuO_x were deposited on a variety of different supports, utilizing the same manufacturing procedure for all supports. The reaction was carried out at benign conditions, i.e. in the absence of catalytic amounts of base, at 10 bar O_2 pressure, and at 150 °C, and the acetic acid yield was approximately 100%; analogous to what was observed by Gorbanev et al. [26] for ruthenium hydroxide supported on $Mg_6Al_2(CO_3)(OH)_{16} \cdot 4H_2O$, $MgAl_2O_4$, TiO_2, and CeO_2. In this work, a greater variety of different supports are tested for the selective oxidation to elucidate any trends in activity based on the support properties. We therefore chose support materials with different acid/base, and redox properties. The gas phase RuO_x deposition method allowed the catalyst nanoparticles to be highly dispersed and relatively homogeneous in size and properties across the variation in supports without adapting the deposition route. This combination enabled direct comparison of the catalytic activity between the different supported catalysts. Furthermore, we attempted to elucidate the origin of the promotional effect of cerium oxide.

The reaction mechanism of the related reaction oxidative dehydrogenation of methanol (CH_3OH) to formaldehyde (HCHO), or formic acid (HCOOH) has been studied extensively on RuO_2. Therefore, it serve as an onset to understand CH_3CH_2OH oxidation as the reaction mechanism and reactivity trends are expected to be the same. It has been suggested that three factors influenced the activity toward selective oxidative dehydrogenation of CH_3OH: the amount of high valence state Ru(VI) [30], the degree of hydration (the amount of $Ru(OH)_4$) [31], and the particle size [32]. Li et al. [30] showed that activity could be correlated to the amount of Ru(VI) using a ZrO_2 supported catalyst. The Ru(VI) species were found to be dominant only at low loadings and were stabilized by the ZrO_2 support. Recently, Huang et al. [33] expanded on the this work and found indications from a thorough spectroscopic study, that the highly disperse Ru(VI) formed oxo-compounds ($(O)_2Ru(OH)(OZr)$, $(O)_2Ru(OZr)_2$, and $(O)Ru(OZr)_4$) on the ZrO_2 surface. Of these oxo-compounds the $(O)_2Ru(OZr)_2$—formed between 500 and 900 °C—was the most selective toward methylformate. Yu et al. [31] showed that the dehydration of $RuO_2 \cdot xH_2O$ on carbon nanotubes resulted in a less active catalyst and an increase in the oxidation to formic acid instead of methyl formate (no CO_2 was formed). This was due to the reduced activity for oxidative dehydrogenation, which is the rate-determining step (as determined by Liu et al. [32] from the kinetic isotope effect). Liu et al. [32] observed that for RuO_2 on SnO_2 the selectivity for the partial oxidation of CH_3OH to CH_2O decreased with decreasing particle size. The authors rationalized that small clusters would not easily lose lattice oxygen, which was shown to be a part of the rate-determining step in the reaction. The optimal loading of Ru was determined only based on the surface density to be 3.5 Ru surface atoms/nm^2 support [32]. The activities of RuO_2 on SnO_2, and SiO_2 for the oxidative dehydrogenation of CH_3CH_2OH were also briefly investigated [32]. In this work we have attempted to relate these observations to the selective oxidation of CH_3CH_2OH over the gas-phase deposited RuO_x on the different supports.

2. Experimental

2.1. Materials

All reagents were used as received. Ethanol (CH_3CH_2OH) (99.9%, Kemetyl A/S), acetaldehyde (CH_3CHO) (>99.5%, Sigma–Aldrich), acetic acid (CH_3COOH) (99.8%, Riedel-de Haën AG) and O_2 (99.5%, Air Liquide Denmark), $RuCl_3 \cdot xH_2O$ (99% ReagentPlus, 40–49 wt% Ru, Sigma–Aldrich), $KMnO_4$ (analysis pure, Merck), Dopamine Chloride (Sigma–Aldrich), Degussa P25 TiO_2 (Degussa), hydrotalcite (HT, $Mg_6Al_2(CO_3)(OH)_{16} \cdot 4H_2O$, courtesy of Haldor Topsøe), $MgAl_2O_4$ (spinel, courtesy of Haldor Topsøe), sodium titanate nanotubes ($Na_2Ti_6O_{13}$-NTs) were synthesized as described in literature [34], ZnO (Sigma–Aldrich), γ-Al_2O_3 (Puralox TH100/150, Sasol), WO_3 (Sigma–Aldrich), and CeO_2 (nanopowder – Sigma–Aldrich), CeO_2 (AMR), and $Ce_{0.5}Zr_{0.5}O_2$ (AMR). Millipore water was obtained from a Milli-Q® water system with a water resistivity of 18.2 MΩ cm.

2.2. Catalyst preparation

General details of the catalyst preparation have been reported previously [29] and are described below:

Step 1, functionalization of supports: 1 g of a support (TiO_2, HT, $MgAl_2O_4$, $Na_2Ti_6O_{13}$-NTs, ZnO, γ-Al_2O_3, WO_3, CeO_2, or $Ce_{0.5}Zr_{0.5}O_2$) was suspended in a 20 mM dopamine chloride solution in 30 vol.% MeOH/Millipore water by sonication for 30 min. The powder was recovered by centrifugation at 20,000 rpm for 60 min and decanting the liquid. The powder was washed by re-suspension in Millipore water, centrifugation and decanting the liquid anew; the washing procedure was repeated 4 times. The resulting powder was finally dried overnight in air at 95 °C. Around 90% of the total mass of the functionalized support were recovered.

Step 2, RuO_x coating: 0.5 g of functionalized support was placed in a glass tube (4 mm in diameter by 30 cm in length) between two pyrex wool plugs in both ends of the tube. The tube was placed, through a septum, in a three-neck flask. A fritted glass tube was also fitted, through a septum, in the three-neck flask and then connected to nitrogen gas with a needle valve to adjust the nitrogen flow (further setup details are given in [29]). 40 mg $RuCl_3 \cdot xH_2O$ was transferred to the flask with 10 ml Millipore water, and the solution was then stirred for ca. 5 min. Then 80 mg $KMnO_4$ was transferred to the flask with another 10 ml Millipore water and the flask sealed. As the formed RuO_4(g) is toxic this was carried out in a fumehood. A flow of N_2 was then introduced through the reaction mixture and the flow adjusted so that the functionalized support was gently flowing in the tube. The flask was continuously stirred at 400 rpm throughout the deposition. Every hour the tube with the catalyst was rotated allowing for a homogeneous coating. After 4 h the deposition was considered finished and the powder collected and used without further preparation. Around 84% of the total mass of the support could be recovered, the rest was lost through the two pyrex wool plugs during the deposition, optimizing these could increase the yield significantly.

For samples with lower ruthenium loading, the amount of $RuCl_3 \cdot xH_2O$ and $KMnO_4$ were halved and for higher loading the amounts were doubled compared to the procedure described above. For the study of heat-treatment effects three samples of 0.3 g of the 1.8 wt% RuO_x/CeO_2 catalyst were heated to 170, 200 and 450 °C, in air for 18 h. All other catalysts were tested without any heat-treatment.

The RuO_x deposited on TiO_2 was previously investigated by X-ray powder diffraction (XRPD) and X-ray photoelectron spectroscopy [29]. From the XRPD analysis it was determined that the RuO_x nanoparticles were amorphous. The valence state of the RuO_x was determined by XPS to be a mixture of Ru(VI) and Ru(III) or $Ru(OH)_4$ [29]. Whether the catalyst contained Ru(III) or $Ru(OH)_4$, and the level of hydration could not be determined by XPS, hence, we use the notation "RuO_x" to describe the mixed oxide/hydroxide. The effect of heat-treatment on the RuO_x/TiO_2 catalyst was also investigated by XPS. Calcination at 250 °C resulted in a dehydration of the RuO_x into a mixed oxide/hydroxide consisting of RuO_2

and Ru^{3+} or hydrated RuO_2 [29]. Furthermore, it was shown that the functionalization of the support with the dopamine chloride played a key role in the deposition of RuO_x, as it did not occur on the pure supports [29].

2.3. Catalyst characterization

Surface areas were determined by nitrogen physisorption measurements at liquid nitrogen temperature on a Micrometrics ASAP 2020. The samples were out-gassed in vacuum at 150 °C for 6 h prior to measurements. The total surface areas were calculated according to the BET method.

X-ray fluorescent (XRF) measurements were used to determine the elemental composition using a PAN'alytical MiniPal 4. The MiniPal software (V. 0.6.B) used the built-in "standardless" peak fit program to evaluate the peak areas. The measurements were calibrated to a series of samples of $RuCl_3 \cdot xH_2O$ impregnated onto CeO_2 powder in the concentration interval of interest.

Scanning Electron Microscopy (SEM, FEI Quanta 200 F) was performed on the uncoated samples dropcast from CH_3CH_2OH suspension directly onto the sample holder. Images were obtained at 5 kV acceleration with the secondary electron emission detector.

Scanning Transmission Electron Microscopy (STEM) images were obtained using a probe-corrected FEI Titan 80-300ST TEM. TEM images were acquired using a FEI Tecnai T20 TEM. The Titan microscope was operated in STEM mode at 300 kV accelerating voltage with 70.8 mrad inner detector angle. The powdered samples were dispersed on TEM copper grids coated with a holey carbon film. STEM High Angle Annular Dark Field (HAADF) and Bright Field (BF) images were acquired simultaneously during every scan, thereby providing complementary data for efficient image analysis. STEM HAADF imaging is a technique sensitive to Z contrast and, therefore, particularly suitable for Ru deposition analysis on a variety of substrates. Energy Dispersive X-ray (EDX) spectra were recorded in STEM mode to study the spatial distribution of the catalyst material and the compositional topography of the deposits.

X-ray Photoelectron Spectroscopy (XPS) was applied to determine the surface composition using a Thermo Scientific Theta Probe instrument. The X-ray source is monochromatized Al Kα (1486.7 eV) and the analyzer entrance accepts electrons emitted between 20° and 80° to the surface normal. An X-ray beam size of 400 μm was used and the energy resolution corresponds to Ag 3d5/2 full width half maximum (FWHM) of better than 1.0 eV. The energy calibration is estimated to ±0.1 eV, based on the variation of the C 1s binding energy (BE) around 285.0 eV. The analysis chamber base pressure was 5×10^{-10} mbar, but up to 1×10^{-8} mbar due to sample degassing was accepted for XPS analysis.

The elements present at the sample surfaces were identified by XPS survey spectra. Quantification and evidence for chemical shifts is provided by more detailed spectra of selected lines, which were analyzed using the Avantage software. Spectrum shifts due to charging were determined and corrected by sputtering Au(0) onto the sample for internal reference, which gives an uncertainty of less than 0.3 eV. Deconvolution of the XPS spectra was accomplished using Gaussian–Lorentzian product functions superimposed on a Shirley background. The spin–orbit intensity ratios were fixed according to electron occupancy ($p1/2 : p3/2$ =0.5 and $d3/2 : d5/2$ =0.66) corrected for spectrometer contributions. Due to feature overlap between Ru 3d, Ce 4s, and C 1s, the Ru 3p3/2 was used to identify the amounts of Ru valence states. The Ru 3p1/2 could not be fitted due to overlap with Sn 3d lines.

2.4. Catalytic testing

Oxidations were carried out in stirred Parr autoclaves equipped with internal thermocontrol (T316 steel) and a Teflon® beaker insert, 100 ml. In each reaction an autoclave was filled with 10 g of a 5 wt% aqueous CH_3CH_2OH solution. Subsequently, one of the supported 0.9–4.9 wt% RuO_x catalysts (weight percentage given on Ru metal basis) was added (0.06–0.33 g for the different loadings, the amount was chosen to give ca. 0.03 mmol Ru in each run). The autoclave was then pressurized with O_2 (10 bar, ca. 16 mmol) and maintained at 150 °C for a given period of time under stirring (500 rpm). After the reaction, the autoclave was rapidly cooled to room temperature, the reaction mixture filtered immediately and analyzed using High-Performance Liquid Chromatography (HPLC, Agilent Technologies 1200 series, Aminex HPX-87H column from Bio-Rad, 300 mm×7.8 mm×9 μm, flow 0.6 ml/min, solvent 5 mM H_2SO_4, temperature 60 °C). The time-resolved measurements were preformed in batch mode, i.e. each data point corresponds to one experimental run. The HPLC was calibrated for CH_3CH_2OH, CH_3CHO, and CH_3COOH from which the carbon balance was calculated.

2.5. Data processing

The concentrations (mol/L) of CH_3CH_2OH, CH_3CHO, and CH_3COOH from the GC measurements are used to obtain the conversion, yield and selectivity on a carbon basis according to the following equations:

$$Conversion(C) = \frac{c(ethanol)_0 - c(ethanol)}{c(ethanol)_0} \times 100\% = \left(1 - \frac{c(ethanol)}{c(ethanol)_0}\right) \times 100\% \quad (1)$$

$$Yield(Y) = \frac{c(product)}{c(ethanol)_0 - c(ethanol)} \times 100\% \quad (2)$$

$$Selectivity(S) = \frac{Y}{C} \times 100\% \quad (3)$$

As the CH_3CHO is a reaction intermediate when going from CH_3CH_2OH to CH_3COOH it may be a little misleading to put too much emphasis on the selectivity between these product as the ratio may be shifted significantly by changing reaction times. The results presented here are not optimized for the best possible selectivity toward CH_3COOH but to reflect the relative difference between catalyst supports.

3. Results and discussion

A recent study has shown that $Ru(OH)_x$ on CeO_2, prepared by impregnation, showed a product yield close to 100% for the aerobic oxidation of ethanol (CH_3CH_2OH) to acetic acid (CH_3COOH) at 150 °C, and 10 bar O_2 after 3 h [26]. In this study we use these experimental conditions to test the catalytic activity of RuO_x deposited on a variety of metal oxide supports. These catalysts were prepared using our recently published gas-phase synthesis [29]. As this synthesis allows for the deposition of similarly sized nanoparticles across the different supports, it enables a direct comparison of the supports' effect on the catalyst activity.

All catalysts were examined by SEM and STEM in order to investigate the morphology of the support and active particles. Fig. 1 shows the morphology of the 1.8 wt% RuO_x/CeO_2 catalyst, which is representative of the samples. The support morphology was determined from the SEM image (Fig. 1(a)) to be nanoparticulate with rounded particles clustered together in larger particle agglomerates. The individual support particles were approximately 100 nm large on average with a broad size distribution, and the agglomerates were on the micrometer length scale.

From the BF and HAADF STEM images the deposited RuO_x could be identified. RuO_x appeared as bright spots or patches in the

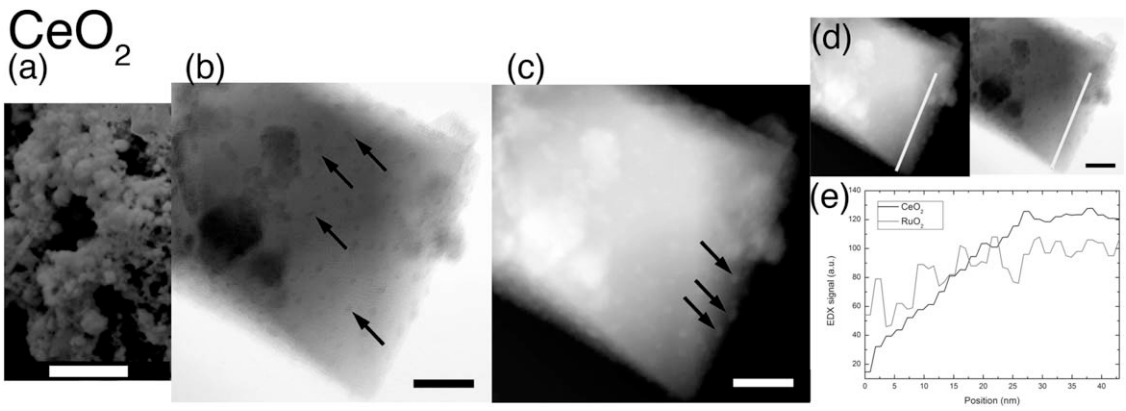

Fig. 1. SEM image (a) and STEM images, in BF (b) and HAADF (c) modes, of the 1.8 wt% RuO_x/CeO_2. (d) The STEM BF and HAADF images showing the EDX linescan position. (e) The EDX linescan of Ru and Ce. The RuO_x particles could be clearly identified from the EDX linescan. The scale bar in (a) corresponds to 500 nm and in (b)–(d) the scale bar corresponds to 10 nm.

HAADF images and dark in the corresponding BF due to its higher atomic number (Z) and indicated by the arrows (Fig. 1(b) and (c)) (on Ce-oxide supports where Ce has a higher Z than Ru, Ru identified by comparing contrast differences in BF and HAADF images). The deposits on the supports surface was confirmed to contain Ru by performing an EDX line scan with a sub-nanometer sized electron probe (Fig. 1(d), line scans for the other samples are not shown). The deposited RuO_x may be seen to consists of individual particles ranging from 0.5 to 1.2 nm in size (estimated from representative STEM images).

From SEM and TEM investigations (see supplementary information), it could be determined that all the catalyst samples contained RuO_x nanoparticles around 0.3–1.5 nm in size, well dispersed on the supporting oxide. As the samples were produced using exactly the same procedure regardless of the supports this was expected. However, this fact also allows for the direct comparison of the supports effect on activity of the RuO_x nanoparticles with only negligible effects of particle size. Table 1 summarizes the observed particle sizes, loading, and the measured BET surface areas. The surface area was seen to vary significantly with the support but seemingly not effecting the catalyst particle size.

The loading of each sample, as measured locally by EDX and in the bulk by XRF, differs significantly (see Table 1), indicating that the supports were inhomogeneously coated with RuO_x. Some smaller variation in the concentration measured by EDX in different areas was observed as is normally the case, hence, a complete agreement between EDX and XRF was not expected, but the observed variations were significantly larger. The inhomogeneity was speculated to be due to either (i) that RuO_4(g) reacts fast with surface dopamine groups resulting in less deposition on particles inside agglomerates, or (ii) to a difference in the surface coverage of dopamine, but most likely a combination of the two. The dopamine molecule was previously shown to be a key participant in the RuO_x deposition mechanism [29]. In the present work it was chosen to adjust the Ru to CH_3CH_2OH ratio to 0.3 on molar basis (mol%, based on the XRF measurements, see Table 1) for all catalysts in the catalytic activity tests to take the variation in loading into account and allow for the direct comparison of the different supports.

In Fig. 2, the various catalysts from Table 1 are compared on the basis of the CH_3COOH yield after 3 h of reaction. The catalyst materials indicated by $*$ in Table 1 showed a carbon mass balance of less than one (measured by HPLC) indicating the full oxidation of CH_3CH_2OH to CO_2 [26,35]. The carbon mass balance varied between 60 and 70% for the indicated samples. The full oxidation to CO_2 could not be verified by the conducted HPLC analysis, but has previously been observed by Imamura et al. [35] for the oxidation of CH_3COOH over a RuO_2/CeO_2 catalyst. In contrast to the work of Imamura et al. [35], the yield of CH_3COOH was close to 100% after 17 h (as seen in Fig. 3). Coke formation, or other insoluble products, that could also have contributed to the deviation in the carbon mass balance, were not detected as the reaction mixtures were filtered before analysis. Most of the catalysts were stable under the employed conditions, with the exception of RuO_x/ZnO, which formed an unidentified foam during the reaction. We expect that this by-product was formed by reaction of amphoteric ZnO with the CH_3COOH, as indicated by the carbon balance being lower than

Table 1
Physical properties of the catalysts compared in this work. Catalysts marked with an $*$ in the table, showed a carbon mass balance of less than one, indicating some complete oxidation to CO_2.

Name/support	Ru loading ([wt.%] XRF)	Ru loading ([wt.%] EDX[a])	BET surface area (m^2/g)	Ru particle size [b] (nm)
RuO_x/TiO_2 $*$	4.9	5.3	54	0.3–1.0
RuO_x/HT[c]	1.5	0.6	5	0.5–1.5
$RuO_x/MgAl_2O_4$ $*$	1.5	3.2	89	0.5–1.0
$RuO_x/Na_2Ti_6O_{13}$-NTs $*$	1.5	1.9	214	~0.8
RuO_x/ZnO $*$	1.3	1.1	9	0.8–1.2
RuO_x/γ-Al_2O_3	1.6	0.4	151	0.6–1.5
RuO_x/WO_3 $*$	1.3	1.9	2	0.8–1.0
RuO_x/CeO_2	0.9	3.3	62	~0.5
RuO_x/CeO_2	1.8	1.9	58	0.5–1.2
RuO_x/CeO_2	3.4	3.8	60	0.6–0.8
RuO_x/hisuCeO_2	2.3	3.8	122	0.8–1.5
$RuO_x/Ce_{0.5}Zr_{0.5}O_2$	0.9	5.2	127	1.0–1.5

[a] Metallic Ru content based on known metal oxide composition, averaged over 2–3 EDX spectra.
[b] The particle size was estimated from representative HRTEM images.
[c] The use of this catalyst material resulted in an unidentified peak in HPLC.

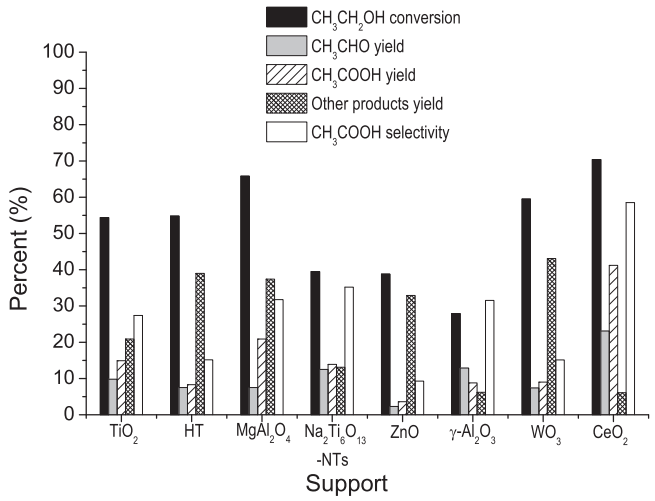

Fig. 2. Conversion, yields, and selectivity for the aerobic oxidation of CH_3CH_2OH with supported RuO_x catalysts (5 wt% aqueous CH_3CH_2OH solution, 10 bar O_2, 150 °C, ca. 0.3 mol% Ru to CH_3CH_2OH, and 3 h of reaction time). Other products are products not detected by the HPLC analysis, i.e. an unknown mixture likely consisting of CO_2 and/or insoluble products.

one. However, it could not be ruled out that the discrepancy of the carbon balance was, at least in part, due to the full oxidation to CO_2.

Generally, it may be seen from Fig. 2 that the TiO_2, $MgAl_2O_4$, and CeO_2 catalysts showed the best performance. The performance of CeO_2 was in line with that observed in literature [27,26] for similar conditions; hence, the rest of this work focuses on the origin of the high activity and selectivity toward CH_3COOH of the RuO_x/CeO_2 catalyst.

The time-resolved reactant, product, and intermediate yields plot is shown in Fig. 3 for the catalytic reaction of the RuO_x/CeO_2 catalyst. This figure shows that, as the CH_3CH_2OH was converted, the amount of CH_3CHO increased together with the CH_3COOH yield. This was expected since it was previously demonstrated that the oxidation of alcohols was more difficult than the oxidation of aldehydes, as is the case for Au on TiO_2 [36,10,37]. Hence, as the CH_3CHO is produced, it is rapidly converted to CH_3COOH. After approximately 2.5 h the yield of CH_3CHO remained almost constant in time, resembling a steady state-like situation. After 12 h, when all the CH_3CH_2OH was converted, the amount of CH_3CHO decreased gradually as the conversion from CH_3CH_2OH to CH_3COOH was completed after about 18 h. This is in contrast to what was observed previously for RuO_2 on SiO_2 and SnO_2 supports [32], where the conversion to CH_3COOH did not occur. It is likely that the difference in reaction conditions were at least partly responsible for this difference, i.e. 0.02–0.5 bar and 100 °C versus 10 bar and 150 °C. Other factors that could affect the selectivity include the particle size, the valence state, the level of hydration, and the crystallinity of RuO_x — these factors were investigated in the following experiments.

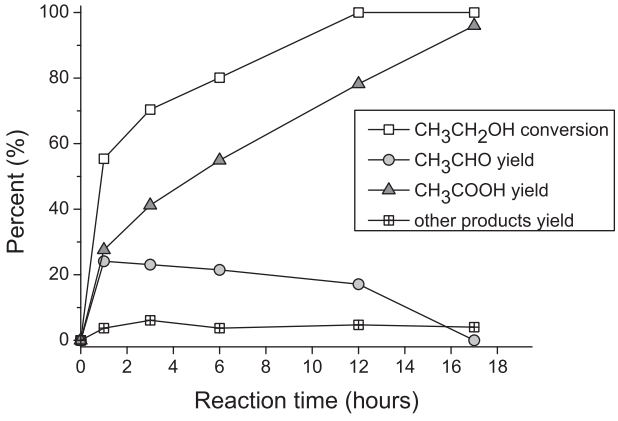

Fig. 3. Conversion of CH_3CH_2OH, and the yields of CH_3CHO, CH_3COOH, and other products as a function of reaction time for the aerobic oxidation of CH_3CH_2OH with 1.8 wt% RuO_x/CeO_2 catalyst in water (5 wt% aqueous CH_3CH_2OH solution, 10 bar O_2, 150 °C, ca. 0.3 mol% Ru to CH_3CH_2OH). Other products are products not detected by the HPCL analysis, i.e. an unknown mixture likely consisting of CO_2 and/or insoluble products.

Liu et al. [32] demonstrated that an optimum in particle size must exist (which they determine as a surface density of 3.5 Ru surface atoms/nm^2 support). To investigate the effect of particle size in the RuO_x/CeO_2 system, the RuO_x loading was increased, which would normally lead to an increase in particle size. This was achieved by varying the amount of Ru-precursor reacted with the support, and loadings of 0.9, 1.8, and 3.4 wt% Ru, were obtained. In Fig. 4 the CH_3CH_2OH conversion and yield of CH_3COOH are shown for the three different loadings.

From Fig. 4 it is seen that, within the experimental uncertainty, there was no difference in catalytic activity with the variation in loading. As the experiments were normalized to the Ru content (ca. 0.3 mol% Ru to CH_3CH_2OH), the similar efficiency was interpreted as an indication of the RuO_x particles having the same size and morphology. In fact, from the STEM images (see supplementary information) and the results summarized in Table 1, it was clearly seen that the particle size did not vary significantly with the loading.

This was in contrast to what is usually been observed for catalysts prepared by impregnation, where particle size most often increases with loading. Thus, this deposition method does not show the normal loading-size dependence. Meaning that the gas-phase deposition synthesis allows for preparing high loadings, while maintaining a small nanoparticle size, without using high surface area supports. This property is a desired feature for a potential industrial process, where a higher loading means a more compact catalyst bed and, correspondingly, smaller equipment. Furthermore, the absence of loading dependence also excludes that the CeO_2 support has an intrinsic activity, in contrast to what was observed by Gorbanev et al. [26]. We attribute this to the dopamine functionalization covering the support or the high dispersion of the RuO_x deposits reacting more efficient than the support. To test further whether the deposited RuO_x activity was not correlated with the loading, a catalyst sample was prepared on high surface area CeO_2 (RuO_x/hisuCeO_2). The surface area of the support was 122 m^2/g compared to 60 m^2/g for the regular CeO_2, and the obtained loading of the catalyst was 2.3 wt%. In Fig. 4 the CH_3CH_2OH conversion and CH_3COOH yield obtained using the RuO_x/hisuCeO_2 are compared to those catalysts prepared with the regular CeO_2; however, no significant difference in catalytic activity was observed. Note that no difference should be observed if the active catalyst particles are similar, as the amount of catalyst used was normalized to the amount of RuO_x. The slightly higher yield of CH_3COOH after 1 and 3 h with the high surface area supported RuO_x compared to the regular CeO_2 supported catalyst may be ascribed to the difference in dispersion of the catalyst in the solution, i.e. differences in mass transport to the catalyst or simply measurement uncertainties.

It should be noted that the time to reach full conversion for all catalysts described here was slightly longer than that observed in literature for catalysts made by incipient wetness impregnation with 1.2 wt% loading — but slightly faster than that with 2.4 wt% loading (normalized to the amount of Ru) [26]. This was likely due to either the difference in particle size, in valence state (which was determined to be mainly Ru(IV) with small amounts of Ru(III) for the incipient wetness impregnated catalysts), or the level of hydration, which is unknown in both cases [26]; all of which could contribute significantly to the activity.

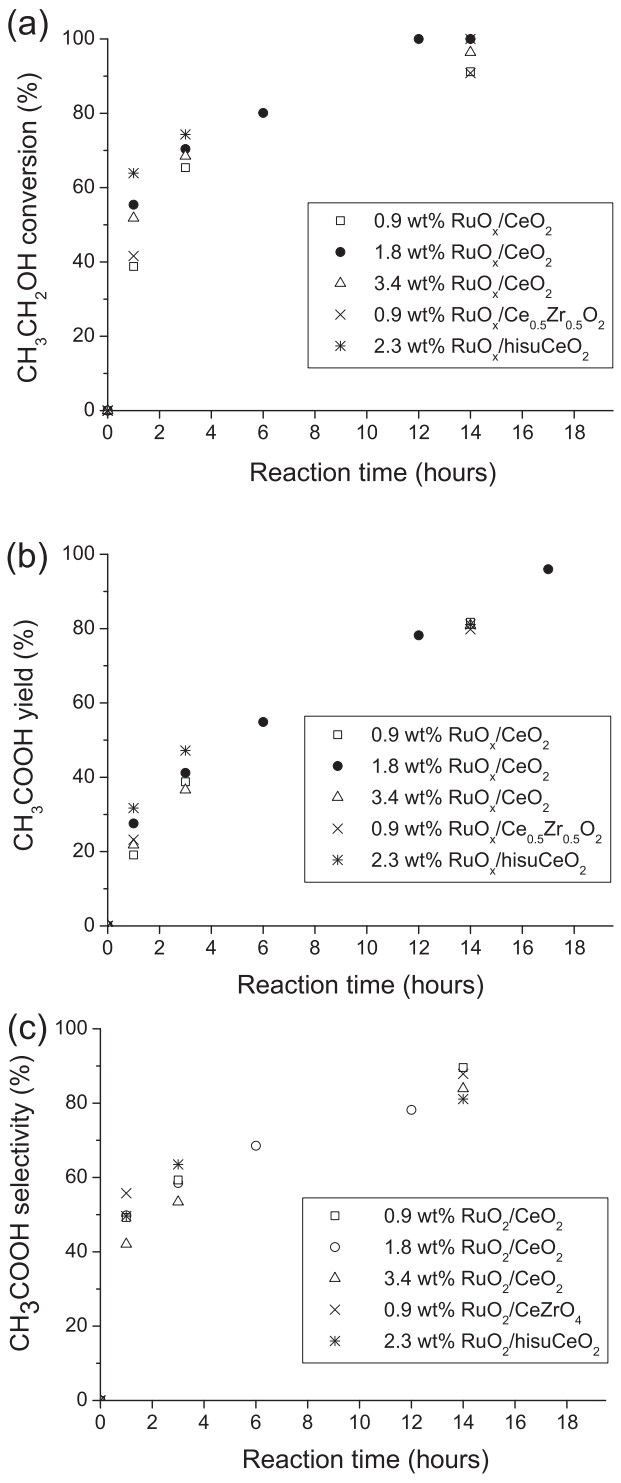

Fig. 4. (a) The conversion of CH_3CH_2OH, (b) the yield of CH_3COOH, and (c) the selectivity toward CH_3COOH in the aerobic oxidation reaction of CH_3CH_2OH with supported RuO_x catalysts (5 wt% aqueous CH_3CH_2OH solution, 10 bar O_2, 150 °C, ca. 0.3 mol% Ru to CH_3CH_2OH).

The particle size observed for the incipient wetness impregnation was around 0.5–2 nm for the most active samples and 0.8–3.5 nm for the sample with comparable activity to that observed in this work [26]. As the particle size range in this study was 0.5–1.5 nm it was not possible to determine an optimal size range from this data. Further studies with well-controlled narrow size-distributions, and valence state are needed to determine how these parameters affect the catalyst activity and to what extent.

Based on literature we speculate that there might two reasons for CeO_2's superior activity: Either because of support effects of the CeO_2 support due to the easy reduction of Ce(IV) oxide or two due to a stabilizing effect of CeO_2 on Ru(VI) species as was suggested by Li et al. [30] for RuO_x on ZrO_2.

It is known from investigations of the automotive three-way catalysts that CeO_2 mixed with ZrO_2 supports have improved oxygen storage properties [38,39], i.e. facilitates the reduction of Ce(IV) to Ce(III) at lower temperatures. It was speculated that the Ce(III)/Ce(IV) redox properties of CeO_2 could be responsible for the increased activity of CeO_2 observed here for the oxidation of CH_3CH_2OH. To elucidate this, RuO_x was loaded onto a mixed ZrO_2/CeO_2 support, $Ce_{0.5}Zr_{0.5}O_2$. This support composition is known from literature to allow the reversible reduction of CeO_2 at the lowest reaction temperature [38,39]. Fig. 4 shows the catalytic results for the $RuO_x/Ce_{0.5}Zr_{0.5}O_2$ catalyst compared to the other CeO_2 supported catalysts. No positive effect was achieved by using the mixed oxide support. Hence, we must tentatively conclude that the reduced temperature for oxidation/reduction was not the right descriptor to explain the increased activity of CeO_2. *In situ* spectroscopy techniques are needed to rule out the involvement of Ce(III)/Ce(IV) in the reaction mechanism or more relevantly its involvement in the rate-determining step.

Our second hypothesis, that the activity of CeO_2 was due to the abundant presence of high valence Ru was based on the work by Li et al. [30] on CH_3OH. In this study Li et al. demonstrated that on ZrO_2 and at low loadings a high fraction of Ru(VI) was present and that these catalysts showed higher catalytic activity. We suggest that CeO_2 could have similar properties, and we thus investigated the samples with the highest and lowest catalytic activity for the presence of these high valence Ru-species by using XPS. As ZrO_2 was suggested by Li et al. [30] as an efficient support to stabilize Ru(VI) species, we also investigated the $Ce_{0.5}Zr_{0.5}O_2$.

From Fig. 2 it is seen that the ZnO has the lowest activity and from the XPS measurements (see Fig. 5, also see supplementary information for all XPS spectra and fits) it is seen that this sample has a 0.10 fraction of Ru(VI) to Ru(IV) compared to 0.17 for the RuO_x on CeO_2. We ascribe the XPS peak at 464.7 eV to Ru(VI) 3p3/2 [41] and the peak at 462.5 eV to RuO_2 [40], the peak at 459.4 eV is ascribed to a low intensity ZnO auger line. This suggests that the high relative amount of Ru(VI) has a promotional effect on the catalytic activity of toward the selective oxidation of CH_3CH_2OH to CH_3COOH, similar to what Li et al. [30] demonstrated for CH_3OH oxidation. Similarly, the $Ce_{0.5}Zr_{0.5}O_2$ show a similar amount (0.18) of Ru(VI) to that of the CeO_2 sample. As these samples also show an equal activity, on Ru metal basis, this agrees very well with the hypothesis that the promotional effect of the CeO_2 support was due to the presence of a larger amount of Ru(VI) compared to the poorly performing ZnO supported RuO_x.

Finally the effect of a heat-treatment on the RuO_x/CeO_2 catalyst was investigated. In Fig. 6 the effect of the catalyst by heat-treatments (at 170, 200, and 450 °C) on the activity is compared to the untreated sample. As the temperature was increased the yield of CH_3COOH and CH_3CHO dropped significantly, compared to the untreated sample. This drop in activity we attributed to the reduction of the active Ru(VI) species. In our previous study [29] of the heat-treatment effect on RuO_x/TiO_2 it was shown that above 250 °C the treatment led to the reduction of Ru from a mixed oxide of Ru(VI) and Ru(III) or hydrated Ru(IV) into a mixed oxide of dehydrated Ru(IV) and Ru(III) or hydrated Ru(IV) (XPS data did not allow for the distinction between Ru(III) and hydrated Ru(IV)). Thus the deactivation of the catalyst toward the formation of CH_3COOH by the heat-treatment at low temperatures occurs simultaneously with the conversion of Ru(VI) species to Ru(IV). However, our previous work [29] it was observed that the heat-treatment also resulted in sintering of the RuO_x into larger particles, as

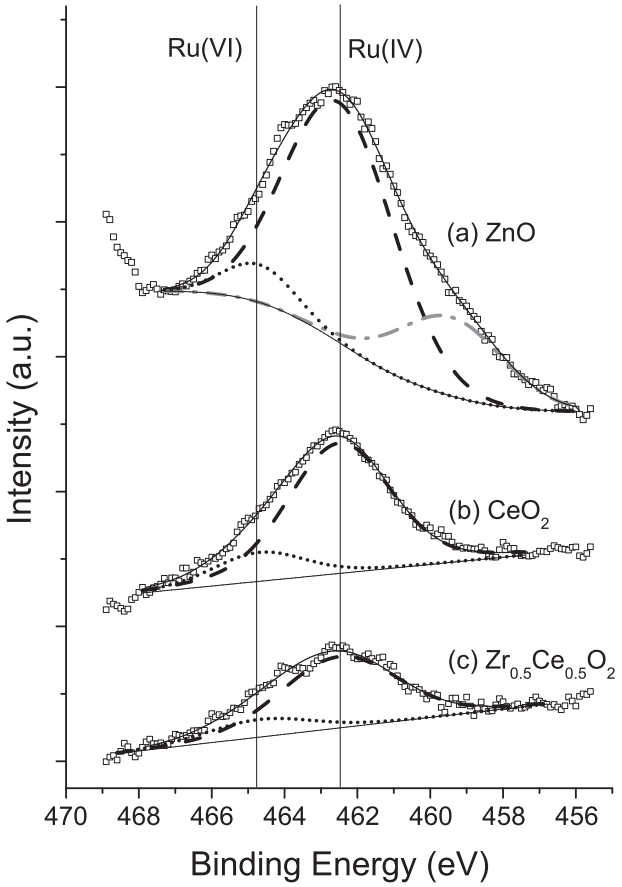

Fig. 5. XPS spectra of the Ru 3p3/2 lines for (a) 1.3 wt% RuO_x/ZnO, (b) 1.8 wt% RuO_x/CeO_2 catalysts, and (c) 0.9 wt% $RuO_x/Ce_{0.5}Zr_{0.5}O_2$. Two lines are observed in both spectra one at 462.5 eV (dashed black line) and one at 464.7 eV (dotted black line), ascribed to Ru(IV) [40] and Ru(VI) [41], respectively. The line at 259.4 eV (dash-dot gray line) in (a) is ascribed to a low intensity ZnO auger line.

determined by TEM (see [29]). This means that from the heat-treatment study alone it was not possible to de-couple the effects of sintering from the change in electronic state, hence, we cannot make any clear conclusions on the relative effect of sintering vs. the reduction/dehydration of Ru(VI). In the study by Liu et al. [32] crystalline RuO_2 on SnO_2 was observed to be more selective toward

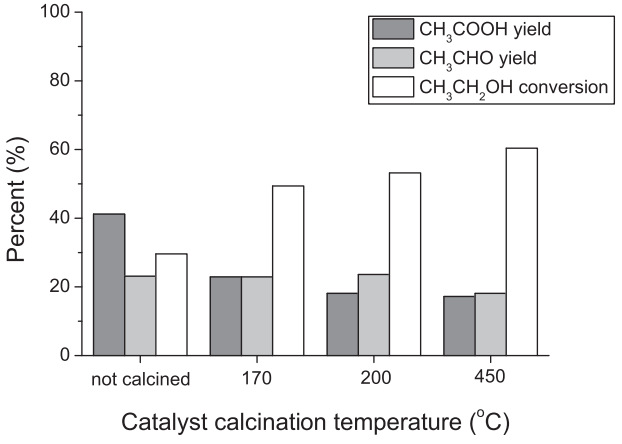

Fig. 6. CH_3CH_2OH conversion, CH_3CH_2HO, and CH_3COOH yields in the aerobic oxidation of CH_3CH_2OH with heat-treated 1.8 wt% RuO_x/CeO_2 catalysts (5 wt% aqueous CH_3CH_2OH solution, 10 bar O_2, 150 °C, ca. 0.3 mol% Ru to CH_3CH_2OH, and 3 h of reaction time).

oxidation of CH_3CH_2OH to CH_3CHO, however, this trend was not observed in the present work.

4. Conclusions

In summary, we have demonstrated that the novel gas-phase synthesis for coating Ru-oxide nanoparticles onto various metal oxides produced active catalysts for the selective aerobic oxidation of CH_3CH_2OH to CH_3COOH. Particles were deposited on P25 TiO_2, $Mg_6Al_2(CO_3)(OH)_{16}\cdot 4H_2O$(hydrotalcite), $MgAl_2O_4$, $Na_2Ti_6O_{13}$ nanotubes, ZnO, γ-Al_2O_3, WO_3, CeO_2 and $Ce_{0.5}Zr_{0.5}O_2$ mixed oxide supports. Of these supports, the CeO_2 proved to be the most active catalyst, followed by the $MgAl_2O_4$, TiO_2, $Na_2Ti_6O_{13}$-NTs, γ-.Al_2O_3, WO_3, HT, and ZnO. To gain insight into the role of the support, we investigated the effect of a CeO_2/ZrO_2 mixed oxide support. As compared to CeO_2, this mixed oxide is known to have increased redox activity in three-way catalysts, but no promotion was observed in the present reaction. On this basis, it was concluded that the activity of CeO_2 supported RuO_x was not influenced by the increased redox activity of $Ce_{0.5}Zr_{0.5}O_2$. From XPS investigations we determined that the most active catalysts stabilized a higher relative abundance of Ru(VI) species as compared to the much less active ZnO supported RuO_x. Furthermore, we have demonstrated that the loading of RuO_x, when deposited by this gas phase reaction, did not effect the catalytic activity when normalized to the RuO_x content. This showed that the nanoparticles deposited by the synthesis are equally active on CeO_2 supports irrespective of the support porosity and catalyst loading. Hence, this type of catalyst may be produced with a very high loading allowing for the use of lesser amounts of catalyst material in a potential industrial process. This could substantially decrease the overall size of an industrial reactor—an important feature for large scale processes.

Acknowledgments

We gratefully acknowledge the assistance of Bodil Holten, CSC, with the BET measurements. This work was funded in part through the Catalysis for Sustainable Energy (CASE) research initiative, which is funded by the Danish Ministry of Science, Technology and Innovation. Center for Individual Nanoparticle Functionality is funded by The Danish National Research Foundation. A.K.S. would like to acknowledge the support from the Hans Christian Ørsted fellowship. The A.P. Møller and Chastine Mc-Kinney Møller Foundation is gratefully acknowledged for their contribution toward the establishment of the Center for Electron Nanoscopy at the Technical University of Denmark.

Appendix A. Supplementary Data

Supplementary data associated with this article can be found, in the online version, at http://dx.doi.org/10.1016/j.apcata.2012.05.025.

References

[1] M. Lancaster, Green Chemistry: An Introductory Text, Royal Society of Chemistry, Cambridge, 2002.
[2] F.S. Wagner, Kirk-Othmer Encyclopedia of Chemical Technology, John Wiley & Sons, Inc, 2002, pp. 115–136.
[3] T.W. Simpson, A.N. Sharpley, R.W. Howarth, H.W. Paerl, K.R. Mankin, J. Environ. Qual. 37 (2008) 318–324.
[4] J. Rass-Hansen, H. Falsig, B. Jørgensen, C.H. Christensen, J. Chem. Technol. Biotechnol. 82 (2007) 329–333.
[5] P. Vinke, W. van der Poel, H. van Bekkum, Stud. Surf. Sci. Catal. 59 (1991) 385–394.
[6] G.-J. ten Brink, I.W.C.E. Arends, R.A. Sheldon, Science 287 (2000) 1636–1639.
[7] T. Mallat, A. Baiker, Chem. Rev. 104 (2004) 3037–3058.
[8] C. Moreau, M.N. Belgacem, A. Gandini, Top. Catal. 27 (2004) 11–30.

[9] C.H. Christensen, B. Jørgensen, J. Rass-Hansen, K. Egeblad, R. Madsen, S.K. Klitgaard, S.M. Hansen, M.R. Hansen, H.C. Andersen, A. Riisager, Angew. Chem. Int. Ed. 45 (2006) 4648–4651.
[10] C. Marsden, E. Taarning, D. Hansen, L. Johansen, S.K. Klitgaard, K. Egeblad, C.H. Christensen, Green Chem. 10 (2008) 168–170.
[11] A. Boisen, T.B. Christensen, W. Fu, Y.Y. Gorbanev, T.S. Hansen, J.S. Jensen, S.K. Klitgaard, S. Pedersen, A. Riisager, T. Ståhlberg, J.M. Woodley, Chem. Eng. Res. Des. 87 (2009) 1318–1327.
[12] Y. Gorbanev, S. Klitgaard, J. Woodley, C.H. Christensen, A. Riisager, ChemSusChem 2 (2009) 672–675.
[13] J.J. Bozell, G.R. Petersen, Green Chem. 12 (2010) 539–554.
[14] S. Kegnæs, J. Mielby, U.V. Mentzel, C.H. Christensen, A. Riisager, Green Chem. 12 (2010) 1437–1441.
[15] A. Köckritz, M. Sebek, A. Dittmar, J. Radnik, A. Brückner, U. Bentrup, M.-M. Pohl, H. Hugl, W. Mägerlein, J. Mol. Catal. A: Chem. 246 (2006) 85–99.
[16] B. Jørgensen, S. Egholm, M.L. Thomsen, C.H. Christensen, J. Catal. 251 (2007) 332–337.
[17] S. Trasatti, Croat. Chem. Acta 63 (1990) 313–329.
[18] A. Klerke, S.K. Klitgaard, R. Fehrmann, Catal. Lett. 130 (2009) 541–546.
[19] P. Schwab, R.H. Grubbs, J.W. Ziller, J. Am. Chem. Soc. 118 (1996) 100–110.
[20] K. Rovik, S.K. Klitgaard, S. Dahl, C.H. Christensen, I. Chorkendorff, Appl. Catal. A 358 (2009) 269–278.
[21] M. Pagliaro, S. Campestrini, R. Ciriminna, Chem. Soc. Rev. 34 (2005) 837–845.
[22] H.-B. Ji, K.K. Ebitani, T. Mizugaki, K. Kaneda, Catal. Commun. 3 (2002) 511–517.
[23] K. Mori, S. Kanai, T. Hara, T. Mizugaki, K. Ebitani, K. Jitsukawa, K. Kaneda, Chem. Mater. 19 (2007) 1249–1256.
[24] N. Mizuno, K. Yamaguchi, Catal. Today 132 (2008) 18–26.
[25] F. Nikaidou, H. Ushiyama, K. Yamaguchi, K. Yamashita, N. Mizuno, J. Phys. Chem. C 114 (2010) 10873–10880.
[26] Y.Y. Gorbanev, S. Kegnæs, C.W. Hanning, T.W. Hansen, A. Riisager, ACS Catal. 2 (2012) 604–612.
[27] Y. Gorbanev, S. Kegnæs, A. Riisager, Top. Catal. 54 (2011) 1318–1324.
[28] Y. Gorbanev, S. Kegnæs, A. Riisager, Catal. Lett. 141 (2011) 1752–1760.
[29] A. Kleiman-Shwarsctein, A.B. Laursen, F. Cavalca, W. Tang, S. Dahl, I. Chorkendorff, Chem. Commun. 48 (2012) 967–969.
[30] W. Li, H. Liu, E. Iglesia, J. Phys. Chem. B 110 (2006) 23337–23342.
[31] H. Yu, K. Zeng, X. Fu, Y. Zhang, F. Peng, H. Wang, J. Yang, J. Phys. Chem. C 112 (2008) 11875–11880.
[32] H. Liu, E. Iglesia, J. Phys. Chem. B 109 (2005) 2155–2163.
[33] H. Huang, W. Li, H. Liu, Catal. Today 183 (2012) 58–64.
[34] L. Miao, Y. Ina, S. Tanemura, T. Jiang, M. Tanemura, K. Kaneko, S. Toh, Y. Mori, Surf. Sci. 601 (2007) 2792–2799.
[35] S. Imamura, I. Fukuda, S. Ishida, Ind. Eng. Chem. Res. 27 (1988) 718–721.
[36] G. Tojo, M.I. Fernández, Oxidation of Alcohols to Aldehydes and Ketones, Springer, New York, 2006.
[37] G. Tojo, M.I. Fernández, Oxidation of Primary Alcohols to Carboxylic Acids, Springer, New York, 2007.
[38] R.D. Monte, J. Kašpar, J. Mater. Chem. 15 (2005) 633–648.
[39] M. Sugiura, M. Ozawa, A. Suda, T. Suzuki, T. Kanazawa, Bull. Chem. Soc. Jpn. 78 (2005) 752–767.
[40] NIST X-ray Photoelectron Spectroscopy Database, Version 3.5, National Institute of Standards and Technology, Gaithersburg, 2003, http://srdata.nist.gov/xps/.
[41] J. Guo, T. Zhao, J. Prabhuram, R. Chen, C. Wong, J. Power Sources 156 (2006) 345–354.